

**This item is the archived peer-reviewed author-version of:**

Swift electrochemical detection of paraben an endocrine disruptor by  $In_2O_3$  nanobricks

**Reference:**

Qurashi Ahsanulhaq, Rather Jahangir Ahmad, Yamazaki Toshinari, Sohail Manzar, De Wael Karolien, Merzougui Belabbes, Hakeem Abbas Saeed.- Swift electrochemical detection of paraben an endocrine disruptor by  $In_2O_3$  nanobricks

Sensors and actuators : B : chemical - ISSN 0925-4005 - 221(2015), p. 167-171

Full text (Publisher's DOI): <http://dx.doi.org/doi:10.1016/J.SNB.2015.06.026>

To cite this reference: <http://hdl.handle.net/10067/1274630151162165141>

# Swift Electrochemical Detection of Paraben an Endocrine Disruptor

## By In<sub>2</sub>O<sub>3</sub> Nanobricks

Ahsanulhaq Qurashi<sup>a\*</sup>, Jahangir Ahmad Rather<sup>b,d</sup>, Toshinari Yamazaki<sup>c</sup>, Manzar Sohail<sup>a</sup>

Karolien De Wael<sup>b</sup>, Belabbes Merzougui<sup>a</sup>, Abbas Saeed Hakeem<sup>a</sup>,

<sup>a</sup>Center of Research Excellence in Nanotechnology and Department of Chemistry, King Fahd University of Petroleum & Minerals Dhahran 31261, Saudi Arabia

<sup>b</sup>University of Antwerp, Department of Chemistry, Groenenborgerlaan, 171, B-2020, Antwerp, Belgium

<sup>c</sup>Department of Engineering, Toyama University, 3190 Gofuku, Toyama 930-8555, Japan

<sup>d</sup>Department of Chemistry, Sultan Qaboos University, Box 36, Al-Khod 123, Oman

### Abstract

Novel indium oxide (In<sub>2</sub>O<sub>3</sub>) nanobricks have been prepared by template-less and surfactant-free hydrothermal synthesis method and were characterized by X-ray diffraction (XRD), Raman spectroscopy, Photoluminescence (PL) spectroscopy and field emission scanning electronic microscopy (FESEM). The synthesized In<sub>2</sub>O<sub>3</sub> nanobricks were successfully immobilized on the surface of glassy carbon electrode for the detection of *Parabens* (butylparaben). Owing to the unique structure and intriguing properties of these In<sub>2</sub>O<sub>3</sub> nanobricks, the nanostructured thin-film electrode has shown an obvious electrocatalytic activity for the detection of butylparaben (BP). The detection limit (LOD) was estimated as 3s/m and the sensitivity (LOQ) was calculated as 10 s/m and were found to be 0.08 μM and 0.26 μAnM<sup>-1</sup> cm<sup>-2</sup> respectively. This sensor showed high sensitivity compared with the reported electrochemical sensors for the detection of BP. The fabricated sensor was successfully applied for the detection of butyl paraben in real cosmetic samples with good recovery ranging from 96.0% to 100.3%.

**Keywords:** In<sub>2</sub>O<sub>3</sub> nanobricks, synthesis, Electrochemical BP detection

\*Corresponding author email: [ahsanulhaq06@gmail.com](mailto:ahsanulhaq06@gmail.com)

Tel: 00966-03-860-7063

## 34 **1. Introduction**

35  
36 Indium oxide ( $\text{In}_2\text{O}_3$ ) nanostructures are n-type semiconductors having wide band gap  
37 (*ca.*3.6 eV) and are extensively explored in recent years due to their excellent electronic and  
38 optical properties in optoelectronic devices, solar cells, gas sensors and biosensors [1, 2]. Up to  
39 now, various methods (vapor transport and wet chemistry) have been employed for the synthesis  
40 of  $\text{In}_2\text{O}_3$  nanostructures [3, 4]. Compared with the vapor transport methods, the solution based  
41 hydrothermal synthesis is demonstrated to be environmentally benevolent and is able to produce  
42  $\text{In}_2\text{O}_3$  nanostructures in large scale which includes quantum dots, nanowires, nanotubes and 3-D  
43 assembled nanostructures [5].  $\text{In}_2\text{O}_3$  nanostructures have been immensely used for detecting  
44 various chemical species ( $\text{C}_2\text{H}_5\text{OH}$ ,  $\text{HCHO}$  and  $\text{NH}_3$ ) due to their improved sensing properties  
45 [6–9].

46 The European Commission during the conference in June 2012, on “Endocrine  
47 Disruptors (EDCs): Current challenges in science and policy” listed Parabens as category 1  
48 priority phenolic endocrine disruptor substances, based on evidence that they obstruct hormonal  
49 functioning. Parabens are designed as esters of p-hydroxybenzoic acid and are extensively used as  
50 antimicrobial preservatives in food ingredients, cosmetic products (deodorants, antiperspirents,  
51 skin moisturizers, body creams, body sprays and sun care) as well as pharmaceutical preparations.  
52 The parabens present in these products are incessantly released into the aquatic media by  
53 domestic wastewater. Therefore, there is growing concern in relation to their potential long-term  
54 effects on humans and wild life [10–14].

55 Literature survey reveals various techniques for parabens detection, such as high  
56 performance liquid chromatography [15], capillary electrochromatography [16], gas  
57 chromatography [17], flow injection system combined with chemiluminescence [18], solid phase  
58 extraction (SPE) and supercritical fluid extraction (SFE) [19, 20]. Although these techniques have  
59 high accuracy with low detection limits, but they are expensive, time-consuming and due to the  
60 intricacy of the environmental matrices, pre-concentration of the samples are needed for the  
61 analysis [21]. Electrochemical sensors with potential for environmental applications have been a  
62 subject of tremendous interest in recent past [22–24]. Recently nanostructured electrodes attracted  
63 huge attention for ultrafast phenolic compound detection [25, 26]. The present work describes an  
64 unpretentious method based on a thin film electrode consisting of synthesized  $\text{In}_2\text{O}_3$  nanobricks  
65 coated on glassy carbon electrode (GCE) for the detection of trace amounts of BP. This thin film

66 electrode showed an exceptional electrocatalytic activity due to significant drop in the anodic  
67 overpotential and notable improvement of the anodic current of BP compared with the  
68 electrochemical performances obtained at a GCE.

## 69 **2. Experimental**

### 70 *2.1 Synthesis of In<sub>2</sub>O<sub>3</sub> nanobricks*

71 The typical experiment for the synthesis of In<sub>2</sub>O<sub>3</sub> nanobricks involves a 100 mL capacity  
72 autoclave with a Teflon liner filled with InCl<sub>3</sub>·4H<sub>2</sub>O (0.5 mM) dissolved in distilled water  
73 (100 mL). Then, hexamethylene tetramine (HMTA) (10 mM) was added into the autoclave and  
74 the reactive mixture was stirred robustly for 30 min. After stirring autoclave was sealed and  
75 upheld at 150 °C for 14 h in an oven. Then autoclave was cooled down to room temperature  
76 naturally and the light yellow sample was collected and washed several times with ethanol,  
77 acetone and distilled water to eliminate the probable residual ions in the sample. The products  
78 were dried in a vacuum at 80 °C for 4 h and calcined at 400°C to obtain In<sub>2</sub>O<sub>3</sub> nanobricks.

## 79 **3. Results and Discussion**

80 The crystalline structure of the synthesized indium oxide nanobricks was investigated by  
81 X-ray diffraction (XRD) (Shimadzu XRD 6100 Cu K $\alpha$  (0.15419 nm) technique (Figure 1). All the  
82 peaks were indexed to the pure cubic phase with lattice parameter  $a = 1.011\text{\AA}$  (JCPDS No.  
83 89–4595), indicating that pure cubic phase of In<sub>2</sub>O<sub>3</sub> is obtained. The synthesized indium oxide  
84 nanobricks were also characterized by Raman spectroscopy and Photoluminescence (PL)  
85 spectroscopy, which indicates high crystallinity with a large amount of oxygen deficiency of  
86 cubic In<sub>2</sub>O<sub>3</sub> nanobricks (Supporting information).

87 Surface morphological features of indium oxide nanobricks were investigated by field  
88 emission scanning electronic microscope (FESEM) equipped with EDX. Figure 1B (a-d) shows  
89 various FESEM magnification micrographs of In<sub>2</sub>O<sub>3</sub> nanobricks. A panoramic view of FESEM  
90 micrographs shows that the sample consists exclusively of uniform nanobricks without impurity  
91 particles or aggregates. The nanobricks have well defined uniform dimensions with edge length  
92 ranges from 400-600 nm and height ranges from 200-250 nm. The top surface shows some cracks  
93 at the midst of each box might be caused by mass transport across other side surfaces, which also  
94 resulted in fewer nanoparticle formations around each brick. Their edges are sharp and sides and  
95 top surface are extremely smooth.

96 Before sensor fabrication, the GCE surface was polished with PK-4 polishing kit, BASI  
97 MF-2060 consecutively followed by washing systematically with redistilled deionized water until  
98 a mirror like finish was obtained. It was then dipped in a beaker containing 0.2 mol/L H<sub>3</sub>PO<sub>4</sub>  
99 solutions to remove the adhered powder, rinsed with distilled water and dried at room temperature  
100 for 10–15 minutes. Stock solution of indium oxide nanobricks in form of an ink (1.0 mg/mL) was  
101 prepared in 50% dimethyl sulfoxide (DMSO) by ultrasonication for 30 minutes. Then 8 μL of this  
102 solution was deposited onto the surface of GCE using a microsyringe and dried under IR lamp.

103 Electrochemical measurements were performed using a μ–Autolab  
104 Potentiostat/Galvanostat PGSTAT from Metrohm (Netherlands), integrated with a PC provided  
105 with the NOVA 1.8 software. A three-electrode cell was used which consists of In<sub>2</sub>O<sub>3</sub>/GCE as  
106 working electrode, Ag/AgCl as reference electrode and a graphite rod as an auxiliary electrode.  
107 All working solutions for electrochemical measurements were de-aerated for 10-15 min. with  
108 purified nitrogen gas. All pH–metric measurements were made on a Decible DB–1011 digital pH  
109 meter fixed with a glass electrode and a saturated calomel electrode as reference, which was  
110 previously standardized with buffers of known pH [27].

111 The electrode fabrication was characterized by electrochemical impedance spectroscopy  
112 (EIS) and cyclic voltammetry (CV). Nyquist plot of EIS shows semicircle part and diameter of  
113 semicircle equals the charge-transfer resistance ( $R_{ct}$ ). The  $R_{ct}$  value for the  
114 1.0 mM K<sub>3</sub>Fe (CN)<sub>6</sub><sup>3-/4-</sup> redox probe obtained at In<sub>2</sub>O<sub>3</sub>/GCE was 195Ω (Figure 1C (curve c)  
115 was less than 686Ω Figure 1C (curve b) achieved at GCE implied that charge transfer resistance  
116 of the electrode surface decreased and the charge transfer rate increased on the fabrication of  
117 sensor. This may be due to high conductivity and large surface area of the In<sub>2</sub>O<sub>3</sub> nanobricks at the  
118 surface of GCE. This assumption was further verified by studying the cyclic voltammetry (CV) of  
119 redox probe K<sub>3</sub>[Fe(CN)<sub>6</sub>] to characterize the property of modified electrode. Figure 1D shows the  
120 CVs obtained at bare GCE (curve b), In<sub>2</sub>O<sub>3</sub>/GCE, (curve c) in 1.0 mM K<sub>3</sub>[Fe(CN)<sub>6</sub>]. The apparent  
121 microscopic areas of these modified electrodes was calculated using Randles-Sevcik equation;  $i_p$   
122 =  $(2.69 \times 10^5) n^{3/2} AC_0^*D_0^{1/2} v^{1/2}$ . Where  $I_p$  = current maximum in amps,  $n$  = number of electrons  
123 transferred in the redox event,  $A$  = electrode area in cm<sup>2</sup>,  $F$  = The Faraday Constant in C mol<sup>-1</sup>,  
124  $D$  = diffusion coefficient in cm<sup>2</sup>/s,  $C$  = concentration in mol/cm<sup>3</sup> and  $v$  = scan rate in V/s. For  
125 K<sub>3</sub>[Fe(CN)<sub>6</sub>];  $n = 1$  and  $D = 7.6 \times 10^{-6}$  cm<sup>2</sup>/s and the microscopic areas of GCE and In<sub>2</sub>O<sub>3</sub>/GCE  
126 was calculated and was found to be (0.02 cm<sup>2</sup>) and (0.042 cm<sup>2</sup>) respectively. Evidently, the In<sub>2</sub>O<sub>3</sub>

127 modified electrode ( $\text{In}_2\text{O}_3/\text{GCE}$ ) had almost twice the surface area compared to GCE and thus acts  
128 as a better electrocatalyst for the oxidation of BP. Furthermore, negative shift in peak position of  
129  $\text{Fe}^{\text{II}}$  oxidation reveals fast charge transfer on  $\text{In}_2\text{O}_3/\text{GCE}$ , which is same in accordance with EIS  
130 observation.

131  
132 **Figure 1**

133 The electrocatalytic activity of  $\text{In}_2\text{O}_3/\text{GCE}$  sensor for the oxidation of  $2.4 \mu\text{M}$  BP  
134 ( $0.1 \text{ mM}$  BP stock solution in ethanol; BP was purchased from Sigma-Aldrich, Belgium) was  
135 studied in phosphate buffer (pH 7.0) by cyclic voltammetry. A typical CV of BP exhibits a single  
136 well-defined anodic peak at  $0.85 \text{ V}$  (vs.  $\text{Ag}/\text{AgCl}$ ) assigned to the oxidation of phenolic (OH)  
137 group and no corresponding cathodic peak was obtained indicating the irreversibility of electrode  
138 process. The mechanism involves single electron oxidation of phenolic group (OH) of BP, which  
139 results in formation of benzoquinone (Scheme 1). It was also observed that modification of GCE  
140 surface by a thin film of  $\text{In}_2\text{O}_3$  remarkably improved the sensitivity of  $\text{In}_2\text{O}_3/\text{GCE}$  towards the BP  
141 detection. The reason for better performance of  $\text{In}_2\text{O}_3/\text{GCE}$  sensor may due to the nanometer  
142 dimensions of  $\text{In}_2\text{O}_3$ , electronic structure, topological and high surface area of  $\text{In}_2\text{O}_3$   
143 nanostructured thin film. Figure 2 illustrates the voltammograms, CV (Figure 2A) and SWV  
144 (Figure 2B) of  $2.4 \mu\text{M}$  BP at a bare GCE and  $\text{In}_2\text{O}_3/\text{GCE}$  and it is clear that fabricated  $\text{In}_2\text{O}_3/\text{GCE}$   
145 sensor increase the oxidation peak current of BP and also results in decrease of the over potential.  
146 This confirms the electrocatalytic effect of  $\text{In}_2\text{O}_3/\text{GCE}$  for faster and better detection of BP.

147  
148 **Scheme 1**

149 **Figure 2**

150 The quantitative analysis of BP using  $\text{In}_2\text{O}_3/\text{GCE}$  was performed by squarewave  
151 voltammetry (SWV). The SWV peak current was measured as a function of BP concentration at  
152 least three times under the optimized operational parameters (Figure 3). The calibration plot of  
153 concentration versus peak current was found to be linear over the range of  $0.14 \mu\text{M}$  to  $2.4 \mu\text{M}$ .  
154 The detection limit (LOD) was estimated as  $3s/m$  and found to be  $0.08 \mu\text{M}$  and the sensitivity  
155 (LOQ) was calculated as  $10s/m$  and was found to be  $0.26 \mu\text{A nM}^{-1} \text{ cm}^{-2}$  ( $s$  representing the standard  
156 deviation of the peak currents ( $n = 3$ ) and  $m$  is the slope of the calibration curve).

157 **Figure 3**

158 The validation of the developed  $\text{In}_2\text{O}_3/\text{GCE}$  sensor was carried out to evaluate the  
159 selectivity and specificity in presence of some potential interfering substances having similar  
160 structure as BP. Under optimal conditions, the interference test was performed in the presence of  
161 100-fold concentration of various endocrine disruptors' viz., phenol, and bisphenol-A. The  
162 results obtained indicates that they do not interfere on the signals of 2.4  $\mu\text{M}$  BP with RSD value  
163 of 3.5% indicates that the fabricated sensor is suitable for detection of BP. The  $\text{In}_2\text{O}_3/\text{GCE}$  sensor  
164 showed good stability and reproducibility for the detection of BP (Supporting information).

165 The real sample analysis for the detection of BP was done by analysis of commercial  
166 product *True match cream*® (*LOREAL*). A 0.1 g of cream was dissolved in 25 mL of ethanol by  
167 ultrasonic agitation for 30 min and then the sample solution was centrifuged for 10 min in order to  
168 remove the excipients and finally transferred into 100 volumetric flask and make up with  
169 phosphate buffer of pH 7.0 to obtain 10  $\text{mg mL}^{-1}$  solution of cosmetic sample. The amount of BP  
170 present in the cream was determined by standard addition method at the developed sensor  
171  $\text{In}_2\text{O}_3/\text{GCE}$ . According to the peak current, the total concentration of BP was calculated with an  
172 average regression equation, which was found to be 0.53  $\mu\text{M}$  in this 10 time diluted sample  
173 (equivalent to 5.3  $\mu\text{M}$  , 0.12%) and is within the permissible limit of 0.19 % BP in cosmetics  
174 according to the European scientific committee (SCCS) on consumer safety on 22 March 2011  
175 (SCCS/1348/11). The reliability of the proposed method was verified by calculating the recovery  
176 by standard addition method using three different standard samples (0.5, 1.0 and 1.5  $\mu\text{M}$ ). The  
177 average recovery was obtained in the range of 95.8% to 108.5% with the RSD value less than 5%  
178 (Table 1) indicates high accuracy and precision of the developed method for the determination of  
179 BP in cosmetic samples.

180

181

182 **Table 1**

183

184 **4. Conclusion**

185 The present study reports synthesis of the  $\text{In}_2\text{O}_3$  nanobricks by simple and low  
186 temperature hydrothermal method and characterized by FESEM and XRD techniques. A versatile  
187 electrochemical sensor was developed based on deposition of  $\text{In}_2\text{O}_3$  nanobricks on GCE for the  
188 detection of BP and its analytical performance was relatively studied with bare GCE. The

189 obtained results show that a nanocomposite film of In<sub>2</sub>O<sub>3</sub> nanobricks provided notable advantages  
190 over GCE in accomplishing faster response, tremendous electrocatalytic activity, superior  
191 repeatability, lower background current, and low detection limit, which could be accredited to its  
192 larger specific surface area and greater electron transfer rate. The detection limit (LOD) and  
193 sensitivity (LOQ) was found to be 0.08 μM and 0.26 μAnM<sup>-1</sup> cm<sup>-2</sup> respectively. This developed  
194 sensor becomes an on-field realistic device for expedient detection of other phenolic endocrine  
195 disruptors in ecological matrices.

196  
197  
198  
199  
200  
201  
202  
203  
204  
205  
206  
207  
208  
209  
210  
211  
212  
213  
214  
215  
216  
217  
218  
219

220 **5. References**

- 221 [1] G. Shen, B. Liang, X. Wang, H. Huang, D. Chen, Z. L. Wang, Ultrathin  $\text{In}_2\text{O}_3$  nanowires with  
222 diameters below 4 nm: synthesis, reversible wettability switching behavior, and transparent thin-  
223 film transistor applications, *ACS Nano* 5 (2011) 6148–6155.
- 224 [2] R. Yousefi, B. Kamaluddin, Room-temperature PL spectra indicate that they have a potential  
225 application as properties of ZnO nanobelts, *Appl. Surf. Sci.* 255 (2009) 9376–9380.
- 226 [3] A. Vomiero, S. Bianchi, E. Comini, G. Faglia, M. Ferroni, N. Poli, G. Sberveglieri, Nanobelts  
227 of Semiconducting Oxides, *Thin Solid Films* 515 (2007) 8356–8359.
- 228 [4] Z. W. Pan, R.Z. Dai, Z.L. Wang, Gas Sensing with Nano-Indium Oxides ( $\text{In}_2\text{O}_3$ ) Prepared via  
229 Continuous Hydrothermal Flow Synthesis, *Science* 291(2001)1947–11947.
- 230 [5] W. J. Kim, D. Pradhan, Y. Sohn, Fundamental nature and CO oxidation activities of indium  
231 oxide nanostructures: 1D-wires, 2D-plates, and 3D-cubes and donuts, *J. Mater. Chem. A*  
232 1(2013)10193–10202.
- 233 [6] H. Jiang, J. Hu, F. Gu, W. Shao, C. Li, Synthesis and Photocatalytic Properties of a  
234 Polyaniline-Intercalated Layered Protonic Titanate Nanocomposite with a p–n Heterojunction  
235 Structure, *Chem. Commun.* 90 (2009) 3618–3620.
- 236 [7] N. D. Singh, C. Y. Yan, P. S. Lee, Chemical sensing investigations on Zn– $\text{In}_2\text{O}_3$  nanowires,  
237 *Sens. Actuators B* 150 (2010) 19–24.
- 238 [8] J. X. Wang, B. Zou, S. P. Ruan, J. Zhao and F. Q. Wu, Synthesis, characterization, and gas-  
239 sensing property for HCHO of Ag-doped  $\text{In}_2\text{O}_3$  nanocrystalline powder, *Mater. Chem. Phys.* 117  
240 (2009) 489–493.
- 241 [9] B. X. Li, Y. Xie, M. Jing, G. X. Rong, Y. C. Tang, G. Z. Zhang,  $\text{In}_2\text{O}_3$  hollow microspheres:  
242 Synthesis from designed in (OH)(3) precursors and applications in gas sensors and photocatalysis,  
243 *Langmuir* 22 (2006) 9380–9385.
- 244 [10] A. Hossaini, J. J. Larsen, J. C. Larsen, Lack of oestrogenic effects of food preservatives  
245 (parabens) in uterotrophic assays, *Food Chem. Toxicol.* 38(2000) 319–323.
- 246 [11] P.D. Darbre, J. R. Byford, L. E. Shaw, S. Hall, N. G. Coldham, G. S. Pope, Concentrations of  
247 parabens in human breast tumours, *J. Appl. Toxicol.* 23 (2003) 43–51.
- 248 [12] S. Oishi, Decreased excretion of testosterone and alterations in the male reproductive tract  
249 were observed in male rodents after exposure to butyl and propyl parabens but not to methyl and  
250 ethyl parabens, *Arch. Toxicol.* 76 (2002) 423–429.

251 [13] J. P. Routledge, J. Odum, J. P. Sumpter, Some alkyl hydroxy benzoate preservatives  
252 (parabens) are estrogenic, *Toxicol. Appl. Pharm.* 153(1998) 12–19.

253 [14] P. W. Harvey, D. J. Everett, Significance of the detection of esters of p-hydroxybenzoic acid  
254 (parabens) in human breast tumours, *J. Appl. Toxicology* 24(2004)1– 4.

255 [15] M. Thomassin, E. Cavalli, Y. Guillaume, C. Guinchard, Application of a capillary  
256 electrophoresis method for simultaneous determination of preservatives in pharmaceutical  
257 formulations, *J. Pharm. Biomed. Anal.* 15 (1997) 831–838.

258 [16] K. D. Altria, J. Bestford, Main component assay of pharmaceuticals by capillary  
259 electrophoresis *J. Capillary Electrophor.* 3 (1996) 13-23.

260 [17] P. Canosa, D. Perez-Palacios, A. Garrido-Lopez, M.T. Tena, I. Rodriguez, E. Rubi, R. Cela,  
261 Pressurized liquid extraction with in-cell clean-up followed by gas chromatography-tandem mass  
262 spectrometry for the selective determination of parabens and triclosan in indoor dust,  
263 *J. Chromatogr. A* 1161 (2007) 105–112.

264 [18] R. K. Kobos, Enzyme-based electrochemical biosensors, *Trac-Trend. Anal. Chem.* 6 (1987)  
265 6–12.

266 [19] S. Tuncagil, S. Varis, L. Toppare, Design of a biosensor based on 1-(4-nitrophenyl)-2,5-di-  
267 (2-thenyl)-1H pyrrole, *J. Mol. Catal. B: Enzym.* 64 (2010) 195–199.

268 [20] R. Kazandjian, A. Klibanov, Regioselective Oxidation of Phenols Catalysed by Polyphenol  
269 Oxidase in Chloroform, *J. Am. Chem. Soc.* 107(1985) 5448–5450.

270 [21] C. B. Jacobs, M. J. Pears, B. J. Venton, Carbon nanotube based electrochemical sensors for  
271 biomolecules, *Anal. Chim. Acta* 662(2010) 105–127.

272 [22] B. J. Sanghavi, W. Varhue, J. L. Chávez, C. Chou, N. S. Swami, Electrokinetic  
273 Preconcentration and Detection of Neuropeptides at Patterned Graphene-Modified Electrodes in a  
274 Nanochannel, *Anal. Chem.* 86 (2014) 4120–4125.

275 [23] B. J. Sanghavi, S. Sitaula, M. H. Griep, S. P. Karna, M. F. Ali, N. S. Swami, Real-Time  
276 Electrochemical Monitoring of Adenosine Triphosphate in the Picomolar to Micromolar Range  
277 Using Graphene-Modified Electrodes, *Anal. Chem.* 85 (2013)8158–8165.

278 [24] B. J. Sanghavi, O. S. Wolfbeis, T. Hirsch, N. S. Swami, Nanomaterial-based electrochemical  
279 sensing of neurological drugs and neurotransmitters, *Microchim. Acta* 182 (2015)1–41.

280 [25] F. Liu Y. Piao J. S. Choi T. S. Seo, Three-dimensional graphene micropillar based  
281 electrochemical sensor for phenol detection, *Biosens. Bioelectron* 50 (2013)387–392.

282 [26] C. Carmen M. Mayorga, L. Hlavata, S. Miserere, A. López-Marzo, J. Labuda, J. Pons,  
283 A.Merkoçi, Bismuth nanoparticles for phenolic compounds biosensing application, Biosens.  
284 Bioelectron. 55 (2014) 3553–59.

285 [27] A. Qurashi, J.A. Rather, K. DeWael, B. Merzougui, N. Tabet and M. Faiz, Rapid microwave  
286 synthesis of high aspect-ratio ZnO nanotetrapods for swift bisphenol A detection, Analyst 138  
287 (2013) 47644–768.

288  
289  
290  
291  
292  
293  
294  
295  
296  
297  
298  
299  
300  
301  
302  
303  
304  
305  
306  
307  
308  
309  
310  
311  
312  
313  
314  
315  
316  
317  
318  
319  
320  
321  
322  
323  
324

325 **Figure and table captions**

326 **Figure 1:** (A) XRD spectrum of  $\text{In}_2\text{O}_3$  nanobricks, (B) low and high magnification FESEM  
327 images of  $\text{In}_2\text{O}_3$  nanobricks, (C) Nyquist plots (Inset: Randles equivalent circuit of the GCE and  
328  $\text{In}_2\text{O}_3/\text{GCE}$  to fit the impedance data) and (D) cyclic voltammograms of 1.0 mM  $\text{K}_3[\text{Fe}(\text{CN})_6]$   
329 obtained at GCE (curve b) and  $\text{In}_2\text{O}_3/\text{GCE}$ , (curve c); scan rate of  $20 \text{ mVs}^{-1}$ .

330 **Figure 2:** (A) Cyclic voltammetric and (B) Squarewave voltammetric behavior obtained at  
331 (a) Blank, (b)  $2.4 \mu\text{M}$  BP at GCE and (c)  $2.4 \mu\text{M}$  BP at  $\text{In}_2\text{O}_3/\text{GCE}$ ; scan rate  $20 \text{ mVs}^{-1}$ .

332 **Scheme 1:** Mechanism of the oxidation of BP at  $\text{In}_2\text{O}_3/\text{GCE}$  sensor.

333 **Figure 3:** Linearity of squarewave voltammetric peak current of different concentrations of BP at  
334  $\text{In}_2\text{O}_3/\text{GCE}$ , (a) Blank (b)  $0.14 \mu\text{M}$  (c)  $0.39 \mu\text{M}$  (d)  $0.78 \mu\text{M}$  (e)  $1.04 \mu\text{M}$  (f)  $1.45 \mu\text{M}$   
335 (g)  $1.98 \mu\text{M}$  (h)  $2.4 \mu\text{M}$  ; Inset a calibration graph represents the variation of current with the  
336 concentration of BP. The error bars shows the standard deviation obtained for three separate  
337 experiments.

338 **Table 1:** Recovery studies of BP by standard solutions in cosmetics using fabricated sensor ( $n=3$ )  
339

340

341

342

343

344

345

346

347

348

349

350

351

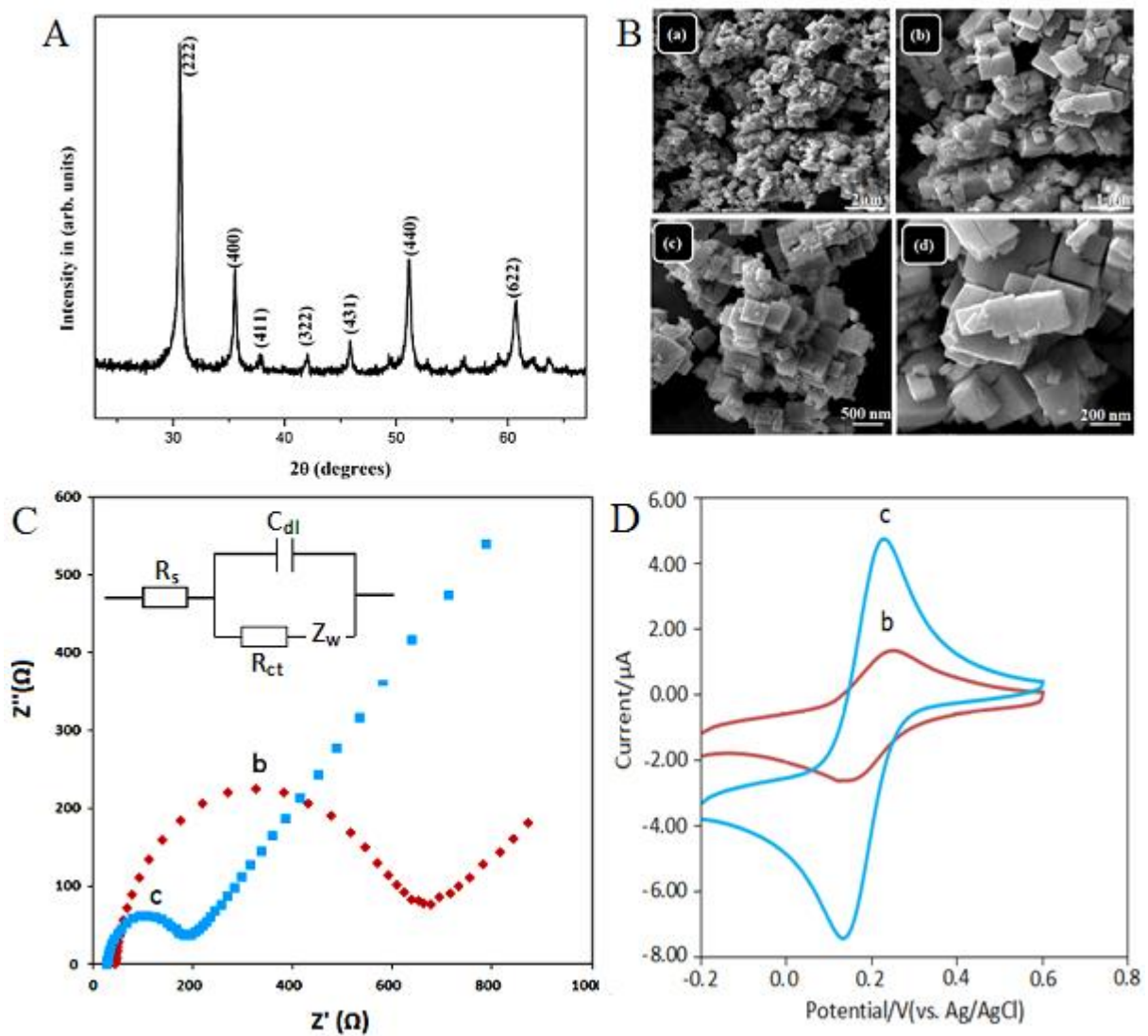
352

353

354

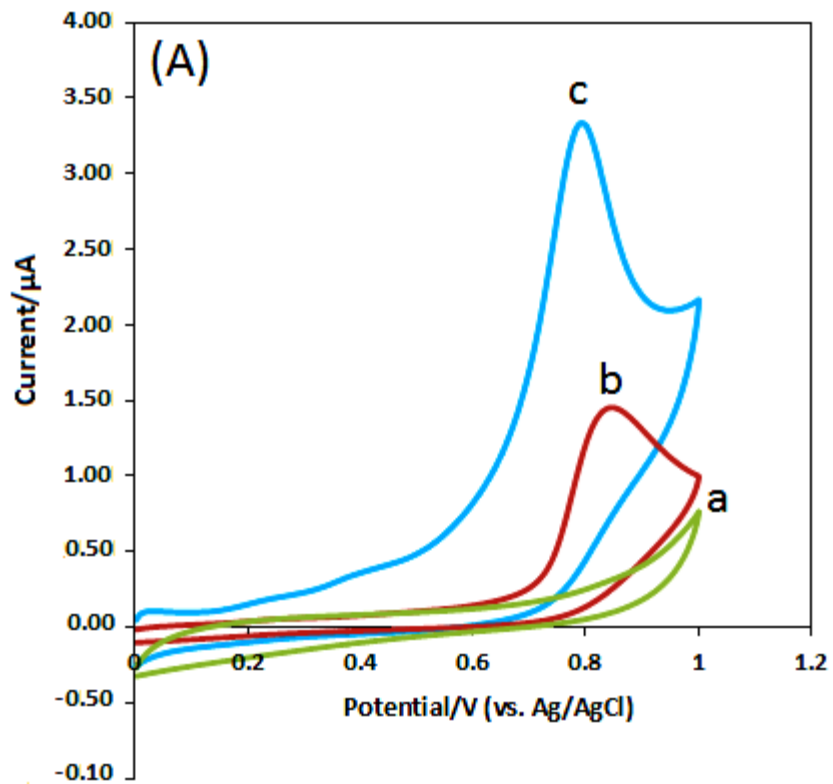
355

356  
357  
358

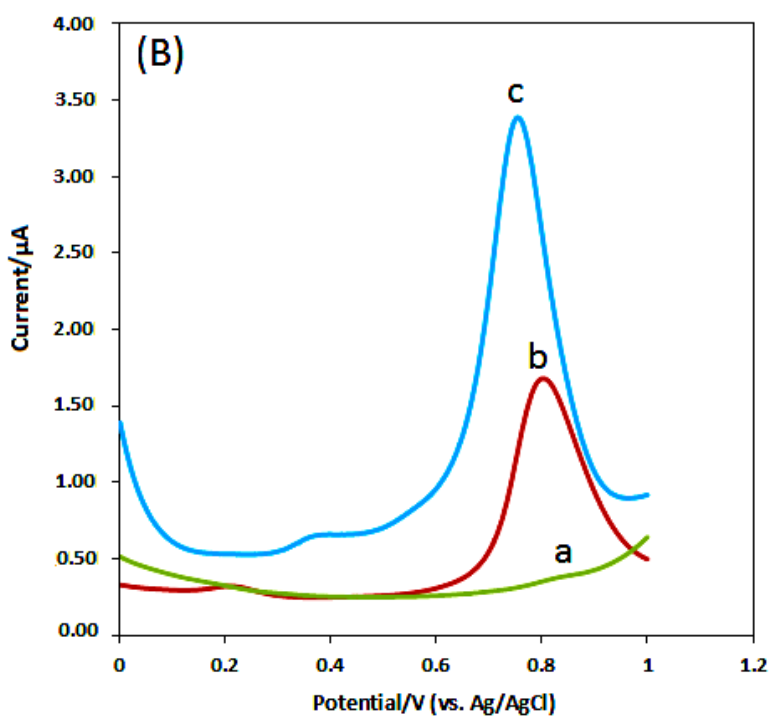


359  
360  
361  
362

Figure 1



363



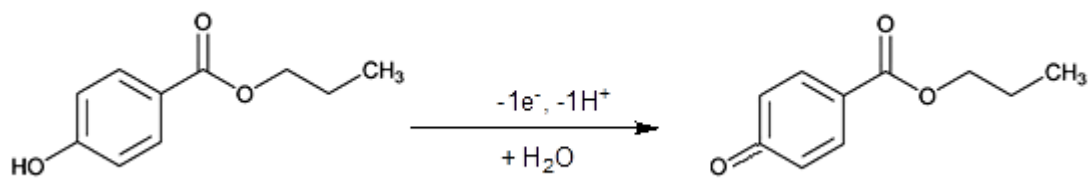
364

365

366

Figure 2

367  
368

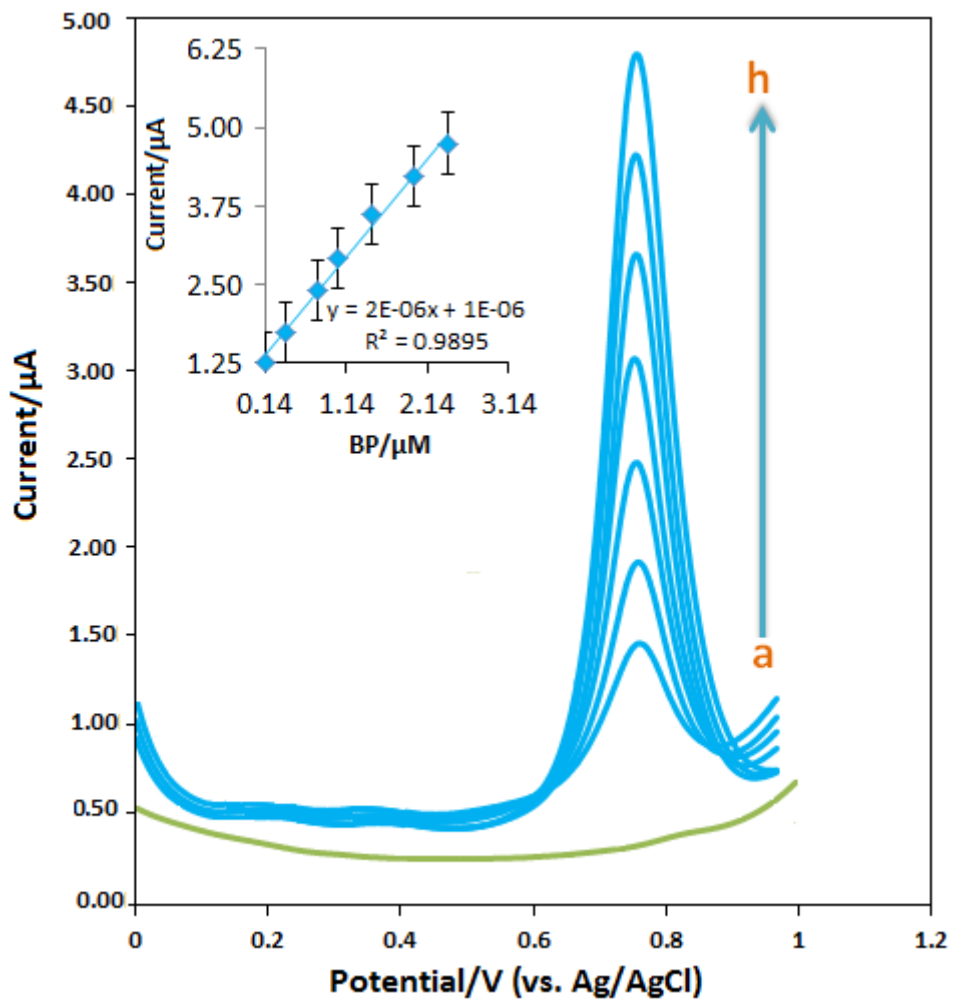


369  
370  
371  
372  
373  
374

**Scheme 1**

375  
376  
377  
378  
379  
380  
381  
382  
383  
384  
385  
386  
387  
388  
389  
390  
391  
392

393  
394  
395



396  
397  
398  
399  
400  
401  
402  
403  
404  
405

Figure 3

406 **Table 1**

Sample	Added ( $\mu\text{M}$ )	Found <sup>a</sup> ( $\mu\text{M}$ )	Actual ( $\mu\text{M}$ )	RSD %	Recovery %
<i>True match Cream</i>	0	0.512	--	2.2	---
<i>True match Cream</i>	0.5	0.970	1.012	3.4	95.8
<i>True match Cream</i>	1.0	1.461	1.512	3.1	96.6
<i>True match Cream</i>	1.5	2.185	2.012	4.9	108.5

407 <sup>a</sup>average of three replicates

408

409